Title

StarD7 Protein Deficiency Adversely Affects the Phosphatidylcholine Composition, Respiratory Activity, and Cristae Structure of Mitochondria*

Journal

Journal of Biological Chemistry, 291(48)

ISSN

0021-9258

Authors

Horibata, Yasuhiro
Ando, Hiromi
Zhang, Peixiang
et al.

Publication Date

2016-11-01

DOI

10.1074/jbc.m116.736793

THE JOURNAL OF BIOLOGICAL CHEMISTRY VOL. 291, NO. 48, pp. 24880–24891, November 25, 2016

StarD7 Protein Deficiency Adversely Affects the Phosphatidylcholine Composition, Respiratory Activity, and Cristae Structure of Mitochondria*

Received for publication, May 6, 2016, and in revised form, August 30, 2016 Published, JBC Papers in Press, September 30, 2016, DOI 10.1074/jbc.M116.736793

Yasuhiro Horibata[‡], Hiromi Ando[‡], Peixiang Zhang[§], Laurent Vergnes[§], Chieko Aoyama[‡], Masahiko Itoh[‡], Karen Reue[§¶], and Hiroyuki Sugimoto[‡1]

From the [‡]Department of Biochemistry, Dokkyo Medical University School of Medicine, 880 Kitakobayashi, Mibu, Tochigi, Japan and the [§]Department of Human Genetics, David Geffen School of Medicine and the [¶]Molecular Biology Institute at UCLA, Los Angeles, California 90095

Edited by Dennis Voelker

Phosphatidylcholine (PC) is a major phospholipid of mitochondria, comprising 40–50% of both the outer and the inner membranes. However, PC must be imported from its production organelles because mitochondria lack the enzymes essential for PC biosynthesis. In a previous study, we found that StarD7 mediates the intracellular transfer of PC to mitochondria. Therefore, in this study, we analyzed the contribution of StarD7 to the maintenance of mitochondrial phospholipid content and function using siRNA-mediated knockdown and knock-out (KO) of the *StarD7* gene in HEPA-1 cells. Real time analysis of respiratory activity demonstrated that the oxygen consumption rate and activity of mitochondrial complexes were impaired in *StarD7*-KD cells. To confirm these results, we established *StarD7*-KO HEPA-1 cells by double nicking using CRISPR/Cas9n. As expected, *StarD7*-KD and -KO cells showed a significant reduction in mitochondrial PC content. The ATP level and growth rate of KO cells were notably lower compared with wild-type cells when cultured in glucose-free galactose-containing medium to force cells to rely on mitochondrial ATP production. In KO cells, the level of the MTCO1 protein, a primary subunit of complex IV, was reduced without a concomitant decrease in its mRNA, but the level was restored when StarD7-I was overexpressed. *StarD7*-KO cells showed impaired formation of the mitochondrial supercomplexes and exhibited a disorganized cristae structure, with no changes in optic atrophy 1 protein. These findings indicate that StarD7 plays important roles in maintaining the proper composition of mitochondrial phospholipids as well as mitochondrial function and morphogenesis.

Eukaryotic cells contain a variety of compartments, or organelles, that perform different functions. The lipid bilayer of the organelle membrane is indispensable for both organelle compartmentalization and the biochemical reactions occurring in or on the surface of organelles. For example, lipid synthesis is primarily catalyzed by membrane-bound enzymes, and oxidative phosphorylation requires a membrane to create proton gradient for ATP synthesis. The lipid bilayer of organelles is thus composed of phospholipids that vary depending on their function. The proper composition of phospholipids in the lipid bilayer is critical for maintaining homeostasis and organelle activity.

Cellular phospholipid biosynthesis occurs in some organelles, such as the endoplasmic reticulum (ER),[2] Golgi complex, and mitochondria (1, 2). Therefore, the existence of machinery for dynamic inter-organelle movement of phospholipids via vesicular or non-vesicular pathways has been speculated. Mitochondria contain the sequential enzymes producing phosphatidylglycerol, cardiolipin, and phosphatidylethanolamine (PE) (3). Phosphatidylserine (PS), synthesized in the ER, is transported to mitochondria through restricted membranes called mitochondrion-associated membranes (MAMs), which are transient bridges from the ER to the outer mitochondrial membrane (2). PE is then produced from PS by PS decarboxylase (PSD) in the inner membrane of mitochondria. Unlike the case with PE synthesis, phosphatidylcholine (PC), the major component of both the inner and outer membranes of mitochondria, is thought to be imported from its sites of synthesis, such as the ER or Golgi apparatus, because the sequential enzymes for PC production are not present in mitochondria. However, the precise molecular machinery for PC transport from the ER or Golgi to mitochondria remains obscure.

In yeast, an ER-mitochondria tethering protein complex was recently identified. Mutation of this protein complex impairs phospholipid trafficking between the ER and mitochondria (4).

* This work was supported in part by Grant-in-aid for Young Scientists (B) 25870668 from the Ministry of Education, Culture, Sports, Science and Technology, Japanese Government and U. S. Public Health Services Grant P01 HL028481. The authors declare that they have no conflicts of interest with the contents of this article.

[1] To whom correspondence should be addressed: Dept. of Biochemistry, Dokkyo Medical University School of Medicine, 880 Kitakobayashi, Mibu, Tochigi, Japan. Tel.: 81-282-87-2127; Fax: 81-282-87-2127; E-mail: h-sugi@dokkyomed.ac.jp.

[2] The abbreviations used are: ER, endoplasmic reticulum; PC, phosphatidylcholine; PE, phosphatidylethanolamine; PS, phosphatidylserine; PSD, PS decarboxylase; StAR, steroidogenic acute regulatory protein; START, steroidogenic acute regulatory protein–related lipid transfer; KD, knockdown; MAM, mitochondrion-associated membrane; OCR, oxygen consumption rate; sgRNA, single-guide RNA; SDHA, succinate dehydrogenase complex iron-sulfur subunit A; TFAM, mitochondrial transcription factor A; BN-PAGE, blue native PAGE; Opa1, optic atrophy 1; qPCR, quantitative PCR; BMH, bismaleimidohexane.

A similar mammalian protein complex has been reported, and mitofusin-2 (5, 6), GRP75 (7), Fis1, and Bap31 (8) are known to tether the ER to mitochondria. Loss of these proteins impairs mitochondrial Ca^{2+} uptake from the ER. However, the contributions of these tethering proteins to phospholipid movement between mitochondria and the ER in mammalian cells are not fully understood.

In a previous study, we found an alternative pathway for the transport of phospholipids to mitochondria involving StarD7 (START domain-containing protein) (9). StarD7 is a member of the steroidogenic acute regulatory protein-related lipid transfer (START) domain-containing family. START domains, which contain ~210 amino acid residues, bind to specific lipids, including phospholipids, sterols, and sphingolipids (10–12). We demonstrated that StarD7 specifically binds, extracts, and transfers PC from the donor membrane to the acceptor membrane *in vitro*. There are two variable forms of StarD7, designated StarD7-I, which contains a mitochondrion-targeting sequence in the N terminus, and StarD7-II, which lacks the mitochondrion-targeting sequence. StarD7-I localizes in mitochondria and cytosol, whereas StarD7-II localizes in the cytosol. In HEPA-1 cells, the intracellular transport of exogenously incorporated fluorescent PC into mitochondria is increased when StarD7-I is overexpressed (9). Thus, we concluded that StarD7 is a soluble carrier protein involved in the intracellular transfer of PC to mitochondria. However, the biological functions of this protein in mitochondria are poorly understood.

In this study, silencing and deletion of the *StarD7* gene were employed to clarify the contribution and importance of StarD7 in mitochondrial function. We found that mitochondrial respiration and complex activities were impaired in *StarD7*-knockdown (KD) cells. To confirm these results, we also prepared *StarD7*-knock-out (KO) cells. The mitochondrial PC content was clearly lower in *StarD7*-KD and -KO cells relative to controls, and the ATP level and cell proliferation rate were also lower in KO cells. Surprisingly, *StarD7*-KD and -KO cells showed incomplete formation of cristae. These results suggest that StarD7 plays important roles in PC transfer to mitochondria for maintaining PC homeostasis and mitochondrial function and morphogenesis.

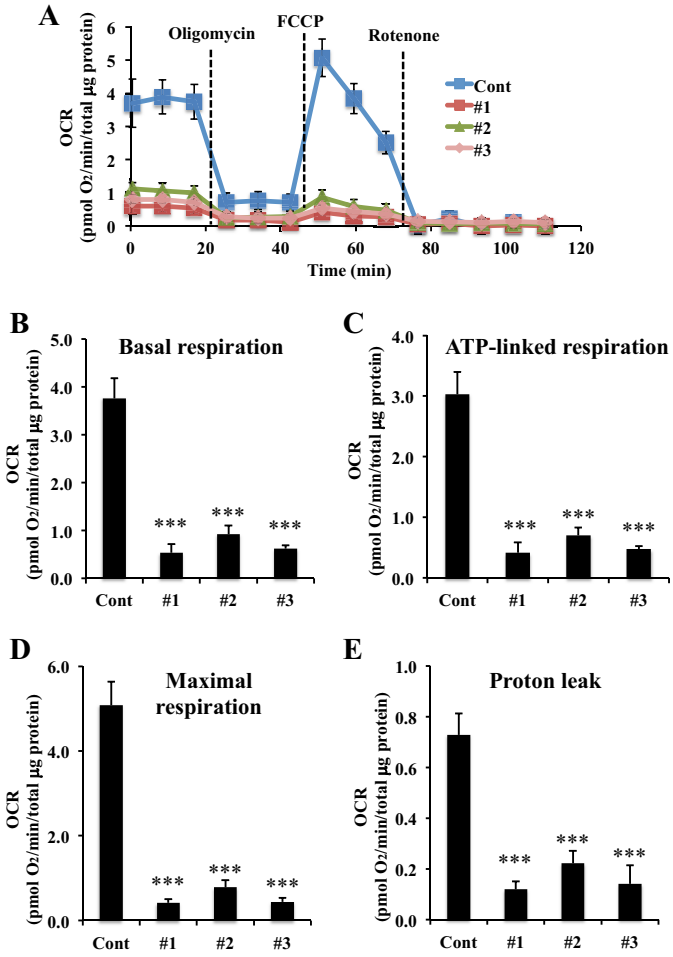

FIGURE 1. **Mitochondrial respiration in HEPA-1 cells was decreased by *StarD7* knockdown with siRNA.** After transfection with three siRNAs against *StarD7* (#1, #2, and #3) or control siRNA (*Cont*), HEPA-1 cells were dispersed on a special Seahorse XF-24 plate and cultured for 1 day before analysis in glucose-free DMEM containing galactose and supplemented with 10% fetal bovine serum. The OCR was determined using a Seahorse XF analyzer in real time. *A,* raw data of OCR. *B,* basal respiration. *C,* ATP-linked respiration (oligomycin-sensitive OCR). *D,* maximal mitochondrial respiration (carbonyl cyanide *p*-trifluoromethoxyphenylhydrazone (*FCCP*)-stimulated OCR). *E,* proton leak. Values are means ± S.D. from four independent culture dishes. Each experiment was repeated more than two times with similar results. ***, $p < 0.001$, as compared with control siRNA.

Results

Acute Reduction in StarD7 Level Following RNAi Silencing Impaired Mitochondrial Respiration—Initially, we reduced the expression of endogenous StarD7 by gene silencing to determine the contribution of this protein to mitochondrial function. HEPA-1 cells were transiently transfected with siRNAs (#1–3) or a control sequence. The three siRNAs target distinct regions of mouse *StarD7* and were obtained from different suppliers. We analyzed the effect of gene KD on real time mitochondrial respiration using a Seahorse XF24 Bioanalyzer (Fig. 1*A*). We thought that ATP generation would be strongly dependent on glycolysis (the Warburg effect), because HEPA-1 cells are derived from a hepatoma. Therefore, to increase the efficiency of ATP generation dependent on mitochondrial oxidative phosphorylation instead of glycolysis, cells were cultured in glucose-free DMEM containing 25 mM galactose 1 day before analysis. *StarD7*-KD cells showed significantly lower basal respiration (Fig. 1*B*), ATP-linked respiration (Fig. 1*C*), maximal respiration (Fig. 1*D*), and proton leak (Fig. 1*E*). We also analyzed the activity of respiratory complexes after permeabilization of intact cells. As shown in Fig. 2, the activity of all mitochondrial complexes in KD cells was significantly impaired.

Next, we determined protein levels in respiratory complexes. In this study, we examined the subunits of complexes II (succinate dehydrogenase complex iron-sulfur subunit B), III (UQCR2, ubiquinol-cytochrome *c* reductase core protein II), IV (MTCO1, mitochondrially encoded cytochrome *c* oxidase I), and V (ATP5A, ATP synthase, mitochondrial F1 complex, α subunit). As shown in Fig. 3*A*, almost no endogenous StarD7 was detected following RNAi silencing. No decrease in protein levels of subunits for these complexes were observed, although the activity of complexes II, III, and V was impaired by *StarD7* KD. In contrast, the level of MTCO1, a primary subunit of complex IV, was significantly reduced in KD cells (Fig. 3*B*).

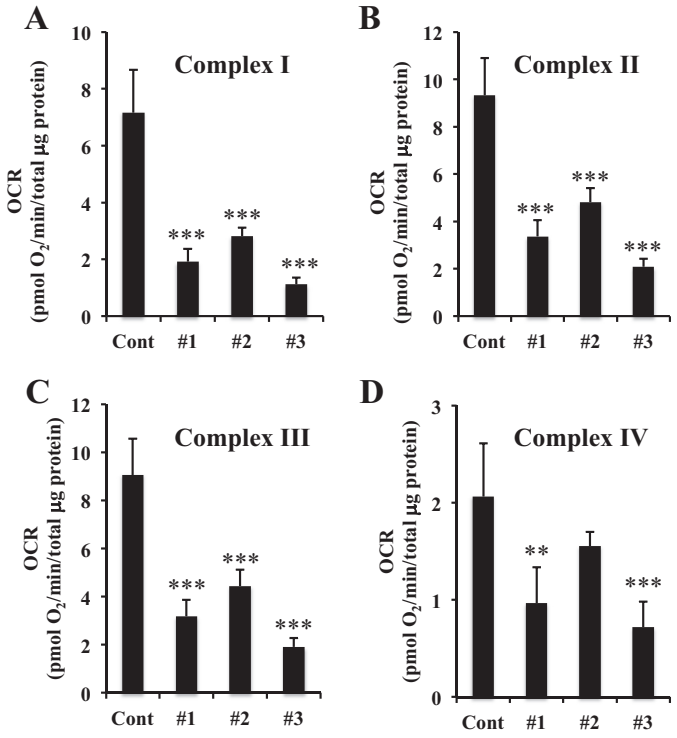

FIGURE 2. **Mitochondrial complex activity in HEPA-1 cells declined following *StarD7* knockdown with siRNA.** After transfection with three siRNAs against *StarD7* (#1, #2, and #3) or control siRNA (*Cont*), HEPA-1 cells were dispersed on a special Seahorse XF-24 plate and cultured for 1 day before analysis in glucose-free DMEM containing galactose and supplemented with 10% fetal bovine serum. To assess mitochondrial complex activity, cells were permeabilized, and mitochondrial complex respiration was determined using a Seahorse XF analyzer in real time. *A,* complex I; *B,* complex II; *C,* complex III; and *D,* complex IV. Values are means ± S.D. from four independent culture dishes. Each experiment was repeated more than two times with similar results. **, $p < 0.01$, and ***, $p < 0.001$, as compared with control siRNA.

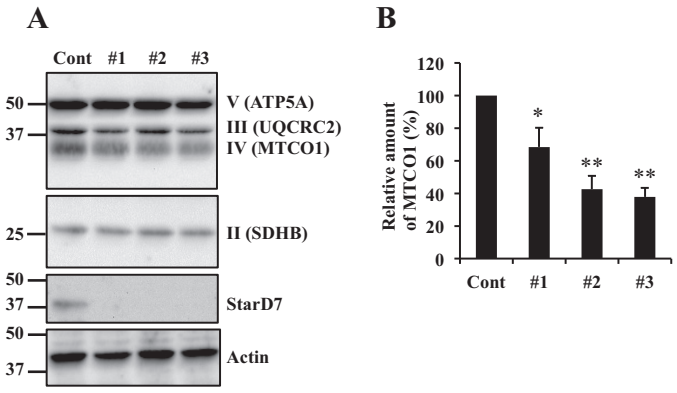

FIGURE 3. **Level of MTCO1 protein declined in HEPA-1 cells after *StarD7* knockdown with siRNA.** *A,* HEPA-1 cells were transfected with three siRNAs against StarD7 (#1, #2, and #3) or control siRNA (*Cont*) and cultured for 3 days in DMEM containing glucose and supplemented with 10% fetal bovine serum. Ten μg of protein were separated by SDS-PAGE, and levels of mitochondrial complex subunit proteins were analyzed by Western blotting. *B,* density of the MTCO1 band in *A* was measured using Quantity One software. β-Actin was used as a loading control. Data were obtained at the linear range of signal intensity. Values are means ± S.D. from three independent experiments. Each experiment was repeated more than two times with similar results. *, $p < 0.05$, and **, $p < 0.01$, as compared with control siRNA.

These findings suggest that StarD7 is required for the activity and stability of respiratory complexes in mitochondria.

Generation of StarD7-KO Cells Using the CRISPR/Cas9n System—To analyze the role of StarD7 in mitochondrial function in more detail, we generated a line of stable HEPA-1 cells in which the *StarD7* gene was ablated using the CRISPR/Cas9 system. To reduce the incidence of off-target ablation, we used a Cas9 double-nickase (Cas9n) method. Approximately 20 colonies were obtained and analyzed after puromycin selection, and 10 clones showed a significant reduction in *StarD7* expression. Genomic DNA was isolated from each of these clones, and DNA regions for both gRNA targets were sequenced. We obtained two clones with deletions in both alleles (Fig. 4, *A* and *B*), and we designated these clones as KO1 and KO2. KO1 showed a 32-bp deletion and 3-bp incorrect insertion, and KO2 showed 20-bp deletions. KO1 cells express mutated StarD7 consisting of a 73-amino acid sequence of the StarD7 N terminus and sequential 19 amino acids of frame-shifted StarD7. KO2 cells express mutated StarD7 consisting of a 69-amino acid sequence of the StarD7 N terminus and sequential 26 amino acids of frame-shifted StarD7. Therefore, both mutated proteins do not contain a START domain (139–328 amino acids). As shown in Fig. 4*C*, a protein band of StarD7 corresponding to molecular mass of about 37 kDa was completely abolished in these KO cells.

StarD7 KO and KD Altered the Mitochondrial Phospholipid Content and Composition—We speculated that the amount of mitochondrial PC might be decreased in *StarD7*-KO cells because StarD7 functions in the transfer of PC to mitochondria (9). Thus, we analyzed the effect of deletion of *StarD7* on the mitochondrial phospholipid content and constitution. Mitochondria were isolated from *StarD7*-KO or wild-type (WT) cells using a Percoll/Nycodenz discontinuous density gradient, and the phospholipids were extracted and analyzed by LC-MS/MS. The purity of the isolated mitochondria was verified by immunoblotting with anti-ATP5A (mitochondria), anti-actin (cytosol), anti-GM130 (Golgi apparatus), anti-PMP70 (peroxisome), and anti-EEA1 (endosome) antibodies (Fig. 5*A*). As expected, the proportion of the major mitochondrial PC, consisting of 18:0–18:1, 16:0–18:1, and 18:1–18:1 fatty acid moieties, was significantly reduced (by 30–40%) in *StarD7*-KO cells compared with WT cells (Fig. 5*B*). For an unknown reason, the proportion of PE with 18:0–18:1 and 18:0–20:4 fatty acid moieties was increased in *StarD7*-KO cells compared with WT cells (Fig. 5*C*). The absolute amounts of major mitochondrial PC (18:0–18:1 and 16:0–18:1) and PE (18:0–20:4) were determined and also decreased in *StarD7*-KO cells compared with WT cells (Table 1). We also quantified mitochondrial PC and PE in *StarD7*-KD cells and confirmed a reduction in PC levels (Fig. 5*D*) and an increase in PE levels (Fig. 5*E*). These results strongly support our previous hypothesis that StarD7 mediates the transfer of PC to mitochondria.

Rescue Experiments of the Reduced Mitochondrial ATP Production and Cell Growth Rate in StarD7 KO Cells—Next, we compared the effect of StarD7 depletion on ATP production and cell growth rate in comparison with WT cells. When *StarD7*-KO cells were cultured in high-glucose DMEM, the ATP level in KO1 cells declined slightly, whereas the ATP level

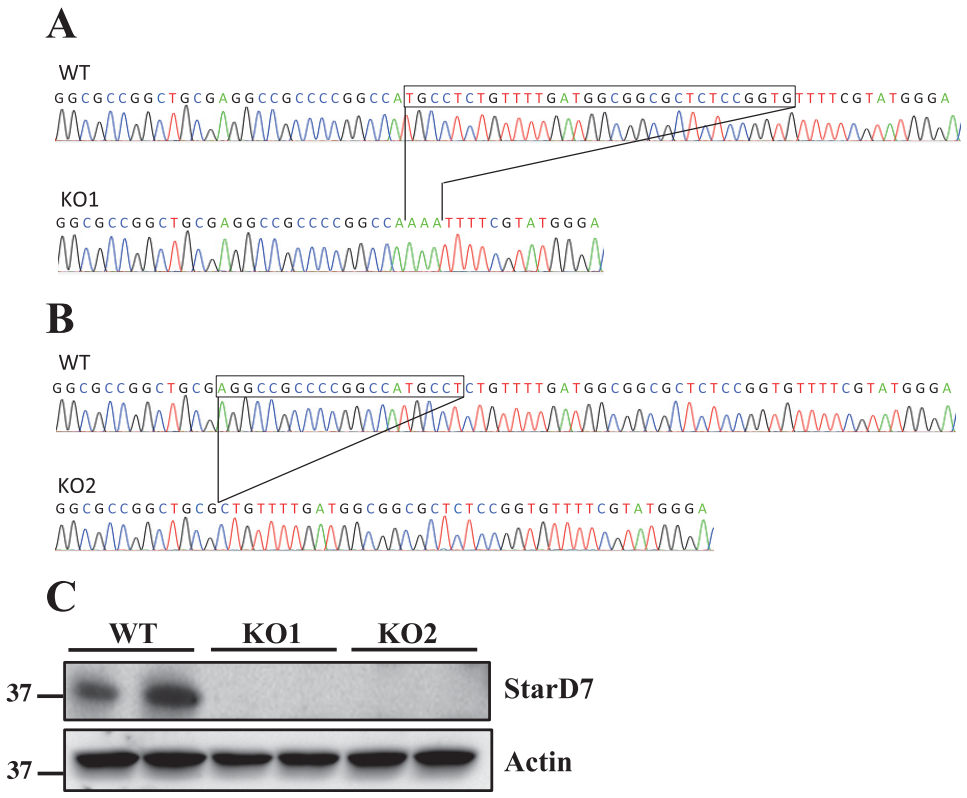

FIGURE 4. **Generation of *StarD7*-KO HEPA-1 cells.** Waveform data from a DNA sequencer displaying the sequence obtained from PCR fragments of genomic DNA from KO1 (*A*) and KO2 (*B*). *C,* protein expression in *StarD7*-KO and wild-type (*WT*) cells was analyzed by Western blotting using an anti-StarD7 antibody. StarD7 expression was completely abolished in *StarD7*-KO cells. β-Actin was used as a loading control.

in KO2 cells was almost the same as that in WT cells (Fig. 6*A*). However, when cells were cultured in glucose-free DMEM containing galactose to force the cells to rely on mitochondrial ATP production instead of glycolysis, the ATP level in *StarD7*-KO cells declined dramatically compared with WT cells (Fig. 6*B*). To confirm that the reduction of ATP production in *StarD7*-KO cells was dependent on the deletion of *StarD7*, we transiently transfected KO cells with a plasmid encoding human *StarD7*-I and -II to rescue StarD7 expression. As we reported previously, there are two variable forms of StarD7, designated StarD7-I, which contains a mitochondrion-targeting sequence in the N terminus, and StarD7-II, which lacks the mitochondrion-targeting sequence (9). StarD7-I therefore localizes in mitochondria and the cytosol, whereas StarD7-II localizes exclusively in the cytosol. As shown in Fig. 6*B*, the reduction of ATP level in *StarD7*-KO cells was partially reversed when StarD7-I was overexpressed in KO cells, but the same effect was not observed with StarD7-II.

We then compared the growth rate of *StarD7*-KO and WT cells cultured in glucose or glucose-free DMEM containing galactose. As shown in Fig. 6*C*, the growth rates were almost the same when the cells were cultured in glucose-containing medium. However, the growth rate of *StarD7*-KO cells was significantly lower than that of WT cells when cultured in glucose-free medium containing galactose (Fig. 6*D*). Cell growth rate of *StarD7*-KO cells in glucose-free medium containing galactose was also rescued when StarD7-I was overexpressed in KO cells as shown in Fig. 6*E*. These results indicate that StarD7 is important for mitochondrial ATP generation and cell growth. These phenotypes of *StarD7*-KO cells were similar to the cells having optic atrophy 1 (Opa1) deficiency, which is an important protein for the maintenance of cristae architecture (13).

Exogenous Expression of Mitochondrial StarD7-I Rescued Levels of MTCO1 Protein—We also determined MTCO1 levels in *StarD7*-KO cells because the level of MTCO1 protein was significantly reduced in *StarD7*-KD cells (Fig. 3). As shown in Fig. 7, the cytochrome *c* oxidase activity of complex IV (Fig. 7*A*) as well as the level of MTCO1 (Fig. 7*B*) were significantly reduced in KO cells. As shown in Fig. 7*B*, the reduction in the level of MTCO1 protein was reversed in part when StarD7-I was overexpressed in KO cells, but the same effect was not observed with StarD7-II overexpression.

StarD7 KO Did Not Reduce Mitochondrial Transcription but Impaired the Formation of Heavy Supercomplexes—Complex IV is composed of 14 protein subunits, 11 of which are encoded by nuclear DNA and 3 of which (MTCO1, MTCO2, and MTCO3) are encoded by mtDNA. To determine why MTCO1 levels were reduced in *StarD7*-KO cells, we quantitatively analyzed the transcription of *MTCO1* using RT-qPCR. In this experiment, we used total RNA treated with DNase to remove mitochondrial DNA prior to PCR. As shown in Fig. 8*A*, levels of *MTCO1* mRNA in KO cells were similar to those in WT cells. We also compared levels of mitochondrial *MTCO3* and *TFAM* mRNA between WT and KO cells. As shown in Fig. 8, *B* and *C*, there were no significant differences between WT and KO cells with respect to levels of these transcripts.

We then examined the effect of *StarD7* KO on the level of mtDNA copy number (*ND1*) relative to nuclear DNA (platelet

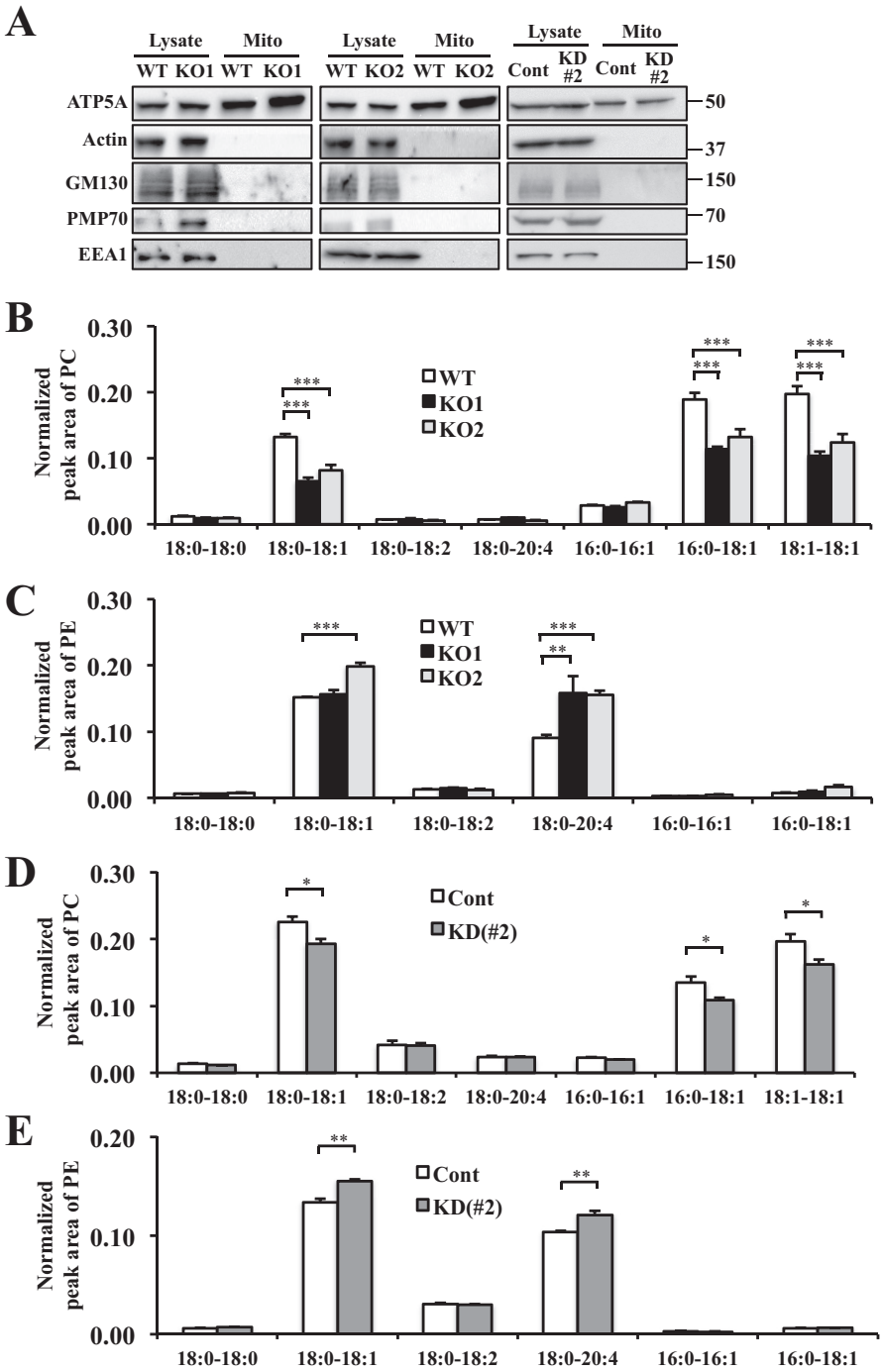

FIGURE 5. **Mitochondrial PC content was reduced and its composition altered in *StarD7*-KO and -KD HEPA-1 cells.** *A*, verification of the quality of purified mitochondria (*Mito*) isolated from *StarD7*-KO and -KD HEPA-1 cells using a Percoll/Nycodenz discontinuous density gradient. Cells were cultured in high-glucose DMEM and transfected with siRNA against StarD7 (#2) or control siRNA (*Cont*) for preparing *StarD7*-KD cells. The whole-cell lysate and mitochondrial fraction were separated by SDS-PAGE and analyzed by immunoblotting using anti-ATP5A (mitochondria), anti-actin (cytosol), anti-GM130 (Golgi apparatus), anti-PMP70 (peroxisome), and anti-EEA1 (endosome) antibodies. *B–E*, phospholipids were extracted from mitochondria from *StarD7*-KO (*B* and *C*) and *StarD7*-KD (*D* and *E*) HEPA-1 cells, and the peak area of PC (*B* and *D*) and PE (*C* and *E*) composed of the indicated fatty acid moieties was determined using LC-MS/MS with multiple reaction monitoring. The peak area for each phospholipid was normalized against the appropriate internal standard. Data are means ± S.D. from quadruple analyses in one experiment. Each experiment was repeated three times with similar results. *, $p < 0.05$, **, $p < 0.01$, and ***, $p < 0.001$, as compared with WT.

endothelial cell adhesion molecule-1, *PECAM-1*). As shown in Fig. 8*D*, there was no significant difference in mtDNA levels between WT and KO cells. Thus, the decrease in the levels of MTCO1 in *StarD7*-KO cells was not the result of a general decrease in mitochondrial transcription.

In *StarD7*-deficient cells, activity of mitochondrial complexes was significantly reduced (Fig. 2). However, protein levels of these complexes were not decreased except complex IV protein, MTCOI (Figs. 3 and 7*B*). To clarify the mechanism for the reduction of complex activity, the formation of mito-

TABLE 1

Quantification of major PC and PE content in mitochondria purified via Percoll-Nycodenz gradient

Values represent means ± S.D. and are expressed as nanomoles/mg protein.

Lipids	WT	KO1	KO2
PC (18:0–18:1)	24.3 ± 0.8	12.1 ± 0.9[a]	15.0 ± 1.5[a]
PC (16:0–18:1)	22.1 ± 1.2	13.4 ± 0.4[a]	15.5 ± 1.4[a]
PE (18:0–20:4)	5.1 ± 0.2	8.8 ± 0.6[a]	8.3 ± 0.8[a]

[a] Values are $p < 0.001$ as compared with WT.

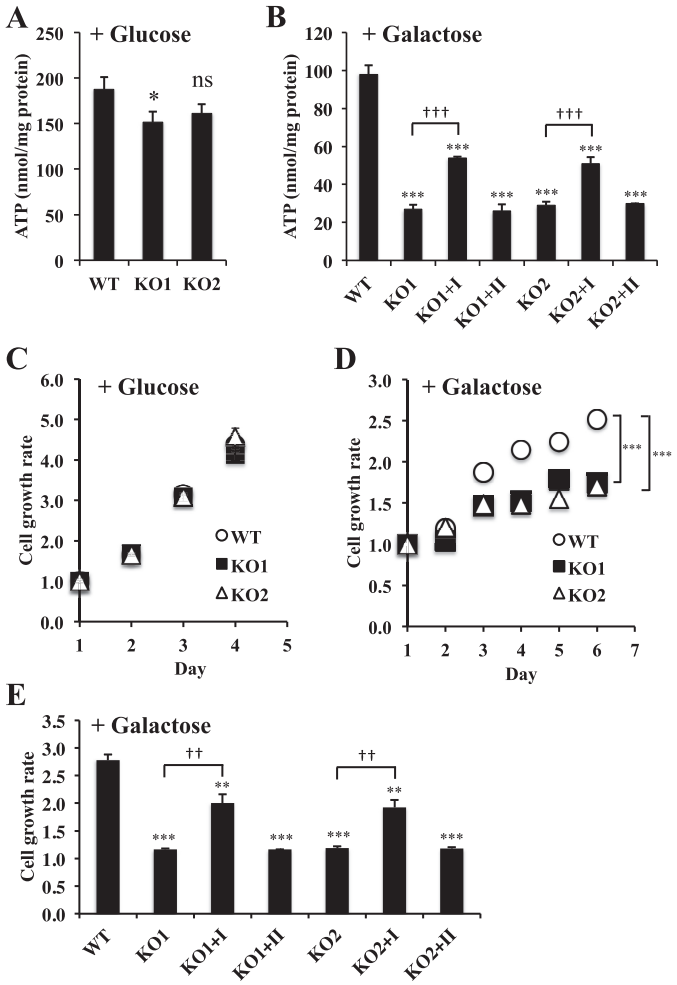

FIGURE 6. ***StarD7*-KO HEPA-1 cells exhibited reduced ATP content and cell growth rate, and overexpression of StarD7-I rescued these defects.** *A* and *B,* wild-type (*WT*), *StarD7*-KO (KO1 and KO2), and KO cells transfected with StarD7-I or StarD7-II (KO1+I, KO1+II, KO2+I, and KO2+II) were cultured in glucose-containing (*A*) or glucose-free DMEM containing galactose (*B*) and supplemented with 10% fetal bovine serum for 24 h. Intracellular ATP content was measured using a luciferin-luciferase-based assay kit, and the results were normalized against protein content. *C* and *D,* cell proliferation rates were determined using a Cell Counting Kit-8 (CCK-8) at 450 nm, according to the manufacturer's protocol. WT, KO1, and KO2 cells were cultured in DMEM containing glucose (*C*) or glucose-free DMEM containing galactose (*D*). *E,* KO cells were transfected with StarD7-I or StarD7-II, and cell growth rate was analyzed after 4 days in glucose-free DMEM containing galactose. Values are means ± S.D. from three independent experiments. Each experiment was repeated more than two times with similar results. *, $p < 0.05$, **, $p < 0.01$, and ***, $p < 0.001$, as compared with WT. †† and ††† indicate significant differences as compared with the cells transfected with empty or StarD7-I containing vector ($p < 0.005$ and $p < 0.001$, respectively). *ns,* not significant.

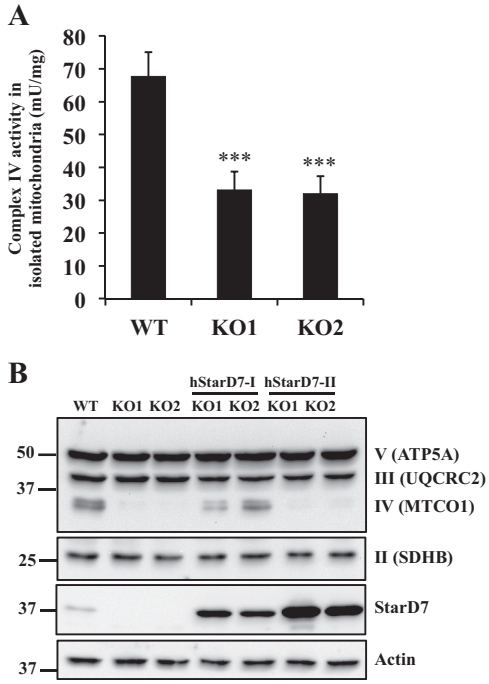

FIGURE 7. **Complex IV activity was reduced in *StarD7*-KO HEPA-1 cells, and overexpression of StarD7-I increased the level of MTCO1 protein.** *A,* mitochondria were isolated from wild-type (*WT*) and *StarD7*-KO (KO1 and KO2) cells using a Percoll/Nycodenz discontinuous density gradient. Cytochrome *c* oxidase activity was analyzed using reduced cytochrome *c* as a substrate. Values are means ± S.D. from four independent experiments. Each experiment was repeated more than two times with similar results. ***, $p < 0.001$, as compared with WT. *B, StarD7*-KO cells were transfected with a plasmid encoding human StarD7-I or StarD7-II and cultured for 3 days. Levels of mitochondrial complex subunit proteins and StarD7 were analyzed by Western blotting.

chondrial supercomplexes was analyzed by blue native-PAGE (BN-PAGE) (14). As shown in Fig. 8*E*, the formation of heavy supercomplexes ($I–III_n–IV_n$) was significantly impaired in *StarD7*-KO cells. From these results, a threshold amount of PC is important for formation and stability of supercomplexes. Next, we analyzed the protein level of SDHA, a catalytic domain of complex II. Even though activity of complex II was reduced (Fig. 2*B*), there was no significant difference in SDHA levels between WT and KO cells (Fig. 8*F*). Thus, the reduction of complex II activity was not due to missing the catalytic subunit.

Loss of StarD7 Alters Mitochondrial Morphology—Next, we examined the effect of *StarD7* deletion on mitochondrial morphology and ultrastructure using electron microscopy. As shown in Fig. 9, *A* and *B*, both control siRNA-treated and WT cells showed intact mitochondrial cristae structures. In contrast, both KD and KO cells lacked normal cristae. These results suggest that StarD7-mediated transfer of PC to mitochondria is essential for the formation of normal cristae.

The inner membrane dynamin-like GTPase Opa1 mediates inner membrane mitochondrial fusion and morphology (13, 15, 16). Inner membrane proteases such as Oma1 cleave long membrane-bound Opa1 forms (Opa1-L) into short soluble forms (Opa1-S). This processing of Opa1 is critical for cristae biogenesis and remodeling (17, 18). Therefore, we examined the abundance and processing of Opa1 by immunoblotting. As shown in Fig. 9*C*, there were no significant differences between WT and KO cells with respect to either the protein level or processing of Opa1. Cristae morphology is also dependent on the oligomerization of Opa1 (13), and oligomerization of Opa1

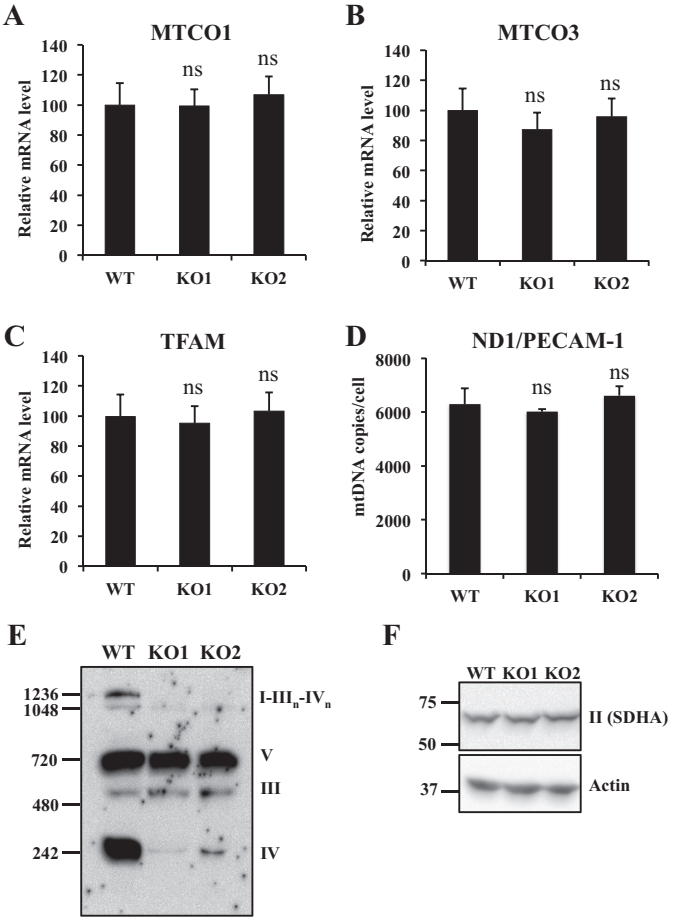

FIGURE 8. ***StarD7*-KO does not affect both mitochondrion-related transcription and mtDNA replication but reduces formation of mitochondrial heavy supercomplexes.** *A–C,* total RNA was isolated from wild-type (*WT*) and *StarD7*-KO cells, treated with DNase I, and used for reverse transcription. Relative levels of *MTCO1* (*A*), *MTCO3* (*B*), and *TFAM* (*C*) mRNAs were determined using RT-PCR. The level of each mRNA was normalized to that of actin (*ACTB*) mRNA. *D,* total DNA was isolated from WT and *StarD7*-KO cells, and the copy number of mtDNA (NADH dehydrogenase 1, ND1) and nuclear DNA (PECAM-1) was determined using RT-PCR. The data were normalized to the copy number of mitochondrial/nuclear DNA. *E,* Western blotting of digitonin-solubilized mitochondria separated on a BN-PAGE with 3–12% acrylamide gradient. Mitochondrial supercomplexes were detected with the total OXPHOS complex antibody mixture. *F,* total cell lysates from WT and *StarD7*-KO cells were analyzed by Western blotting using an anti-SDHA antibody. Values are means ± S.D. from four independent experiments. Each experiment was repeated more than two times with similar results. *ns,* not significant.

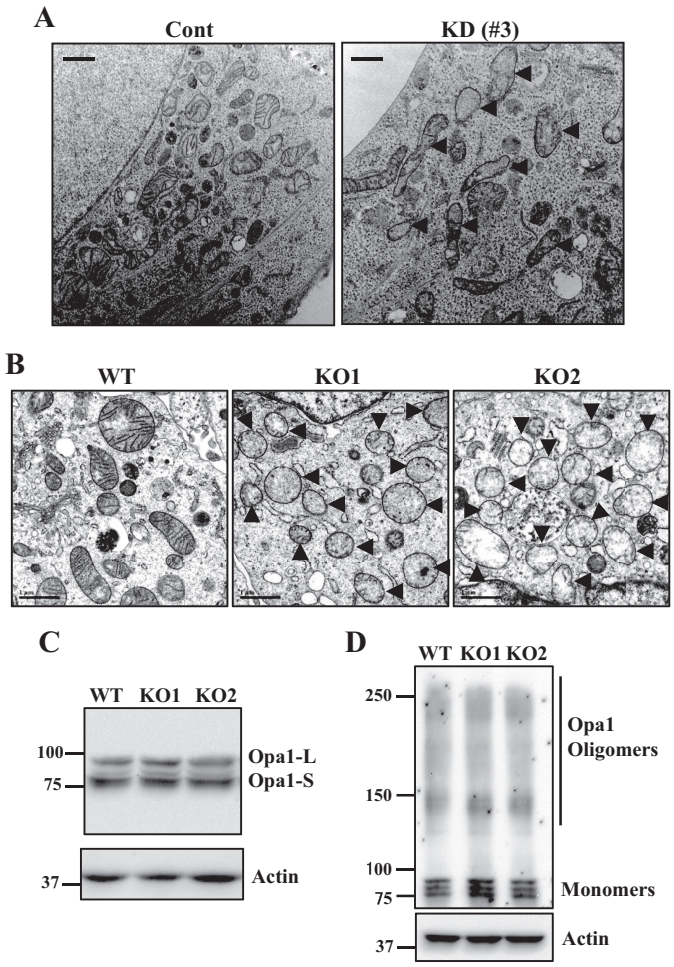

FIGURE 9. **Disruption of normal mitochondrial cristae formation in *StarD7*-KD and -KO HEPA-1 cells.** *A* and *B,* electron micrographs of HEPA-1 cells transfected with siRNAs against *StarD7* (#3) (*right panel, A*) or control siRNA (*Cont*) (*left panel, A*), and WT (*left panel, B*) and *StarD7*-KO cells (*center* and *right, B*). Cells were cultured in high-glucose DMEM. *Scale bar,* 2 μm. *Arrowheads* indicate abnormal mitochondria. *C,* total cell lysates from WT and *StarD7*-KO cells were analyzed by Western blotting using an anti-Opa1 antibody. *D,* cells were treated with BMH, a cell-permeable cross-linker, and oligomerization of Opa1 was analyzed by SDS-PAGE with 5% acrylamide gel and Western blotting using an anti-Opa1 antibody.

was also analyzed. Cells were treated with bismaleimidohexane, a cell-permeable cross-linker, and oligomerized Opa1 was clarified. As shown in Fig. 9*D*, no significant difference in Opa1 oligomerization between WT and KO cells was observed, suggesting that incomplete formation of cristae in *StarD7*-KO cells is independent of Opa1 activity.

Discussion

Although PC is the predominant phospholipid (40–50%) of mitochondria, it must be imported into mitochondria because mitochondria lack the essential enzymes necessary for PC production (2, 3, 19). In our previous study, we showed that the soluble carrier protein StarD7 selectively transfers PC to mitochondria via a mitochondrion-targeting signal at the N terminus and a lipid-transfer domain at the C terminus (9). Here, to further elucidate the role of StarD7 in mitochondrial phospholipid homeostasis, respiration, and morphology, the *StarD7* gene was silenced and deleted.

We found that levels of mitochondrial PC were significantly reduced in both *StarD7*-KO and -KD cells, strongly supporting our hypothesis that StarD7 mediates the transfer of PC to mitochondria. We also found that the enzymatic activity of mitochondrial complexes I, II, and III was significantly impaired in *StarD7*-KD cells, without a concomitant decrease in protein levels. Previously, it was reported that NADH:ubiquinone oxidoreductase (complex I) from bovine heart mitochondria strongly binds to PC and PE and that the enzyme's catalytic activity is dependent on the levels of the bound lipids (20). It was also reported that purified succinate dehydrogenase and succinate-ubiquinone reductase (complex II) interact with PC (21). Moreover, the enzymatic activity of bovine heart mitochondrial ubiquinol-cytochrome *c* reductase (complex III) is affected by the level of PC (22). Therefore, it is likely that

decreases in mitochondrial PC levels adversely affect the activity of these trans-membrane complexes. We found that both the protein level and enzymatic activity of complex IV were significantly reduced by defects in StarD7. As shown in Fig. 8*E*, the formation of mitochondrial heavy supercomplexes ($I–III_n–IV_n$) was significantly impaired in *StarD7*-KO cells. It is reasonable to conclude that post-transcriptional factors impaired the translational mechanism or the stability of the complex, because no reductions in the levels of *MTCO1*, *MTCO3*, and *TFAM* mRNAs or mtDNA were observed in *StarD7*-KO cells. Finally, we found that the structure of mitochondrial cristae was significantly disrupted in *StarD7*-KD and -KO cells. Our results demonstrating impaired mitochondrial complex activity in *StarD7*-KD and -KO cells are in agreement with previous reports indicating that cristae morphology determines the assembly and stability of respiratory complexes (16).

In our previous study, we showed that StarD7 is localized on the outer mitochondrial membrane, where it mediates the transfer of PC to the membrane. However, loss of StarD7 disrupted the inner mitochondrial membrane, impairing cristae formation and the activity of mitochondrial complex enzymes. These results strongly suggest that the phospholipids of the inner membrane are significantly impacted by StarD7. One possible explanation for this is that in addition to transferring PC to mitochondria, StarD7 might also shuttle PC from the outer to the inner membrane within mitochondria. In support of this hypothesis, we can consider the function of StAR, also designated StarD1, another START domain-containing protein. Similar to StarD7-I, StAR has an N-terminal mitochondrion-leading sequence and C-terminal START domain, which can specifically bind to and transfer cholesterol. The outer membrane of adrenal mitochondria contains abundant amounts of cholesterol; however, the inner membrane contains a relatively small amount of cholesterol. Intra-mitochondrial movement of cholesterol from the outer to the inner membrane is the rate-limiting step in steroidogenesis. It is now widely accepted that StAR acts in the intra-membranous space to shuttle cholesterol from the outer to the inner membrane, where it is converted to the first steroid, pregnenolone, by the action of cytochrome P450. To our knowledge, no specific molecules or mechanisms responsible for intra-mitochondrial movement of PC from the outer to the inner membrane have been identified. Thus, the possibility that StarD7 regulates the transfer of PC from the outer to the inner membrane cannot be denied. Further study of the molecular mechanism of StarD7 activity in the intra-mitochondrial space will be needed to resolve this issue.

PE is the second most abundant phospholipid in mitochondria, comprising 35–40% of total mitochondrial phospholipids. Whereas the sequential enzymes for the synthesis of PC are not located in mitochondria, PE can be produced by the action of PSD, which is localized in the inner mitochondrial membrane. Similar to our present findings, another study reported that depletion of mitochondrial PE also causes abnormalities in mitochondrial function (23). Tasseva *et al.* (23) showed that a defect in PSD causing a 20–30% reduction in mitochondrial PE levels also leads to decreases in cell growth rate, respiration and ATP production, and disruption of the structure of cristae in CHO cells. Because PE is a typical cone-shaped lipid that modulates the negative membrane curvature and tends not to form a bilayer during the membrane fusion process (24, 25), a reduction in mitochondrial PE levels might affect mitochondrial inner membrane fusion. Although the importance of PE to proper mitochondrial activity is now better understood, why the deletion of *StarD7* results in disruption of the structure of cristae remains unclear. Opa1 is a mitochondrial GTPase responsible for inner membrane fusion and maintenance of cristae structure. Disorganization of cristae in *StarD7*-KO cells appeared to be independent of Opa1 function, because no changes in either the level or processing of Opa1 protein were observed following deletion. PC exhibits a cylindrical molecular shape and forms flat bilayer structures. In *StarD7*-KO cells, PC levels were about 30–40% lower than in WT cells. Thus, it is possible that the loss of *StarD7* leads to a loss of shortage of PC, disrupting the formation of normal mitochondrial membrane bilayers and thus adversely affecting the mitochondrial structure.

In *StarD7*-KO cells, a significant amount of PC remained in the mitochondria. This result suggests that StarD7 is not the only protein involved in the transfer of PC to mitochondria and that there is an alternative pathway for PC transfer that does not involve StarD7. Other researchers have suggested that the physical bridges between the ER and mitochondria, known as MAMs, are important for the efficient transfer of PS from the ER to mitochondria (2, 26). Although it is not known whether PC is also transferred to mitochondria via MAMs, there are likely several pathways for supplying PC to mitochondria. Further studies involving double KO of *StarD7* and genes encoding ER-mitochondrion-tethering proteins, such as mitofusin-2, GPR75, Fis1, and Bap31, would be useful.

Although we demonstrated that defects in StarD7 reduce the synthesis of cellular ATP *in vitro*, the function of this protein *in vivo* is poorly understood. Yang *et al.* (27) recently generated mice in which one allele of the *StarD7* locus was globally disrupted ($StarD7^{+/-}$ mice) (28). Most $StarD7^{-/-}$ mice died between embryonic days E10 and E11. However, $StarD7^{+/-}$ mice, which express StarD7 at about half the level of WT mice, survived. They also demonstrated increased permeability of epithelial barriers and asthma-like pathological features, such as enhanced allergic responses in the airway and lung. In these tissues, activation of pro-asthmatic myeloid dendritic cells was observed. These results suggest that StarD7 may play an important role in epithelial barrier function and immune homeostasis. Typical mitochondrial dysfunction causes brain, heart, and muscle diseases because of the high energy requirements of these organs. Neurodegenerative disorders or mitochondrial myopathies in *StarD7*-deficient mice require further study, but the results of this study will enhance the general understanding of the pathology and treatment of mitochondrial diseases.

In conclusion, this study demonstrated that StarD7 is non-vesicular carrier that transports PC to mitochondria within cells. StarD7 is indispensable for the maintenance of the proper composition of mitochondrial phospholipids and plays important roles in maintaining the activity, integrity, and stability of mitochondrial complexes and the structure of cristae.

Experimental Procedures

Cell Culture and siRNA-mediated KD—Mouse hepatoma (HEPA-1) cells were cultured in DMEM (high glucose) with 10% fetal bovine serum (FBS) at 37 °C in a humidified incubator containing 5% CO_2. For KD, we used three siRNAs: #1 (GAG AUC AAA GUG AAA GAC UTT) and #2 (GAC AUA CAG UGA CAA UCC ATT) were MISSION siRNAs obtained from Sigma, whereas #3 (CAA GAA CAU GGA GAU CAA AGU GAA A) was Stealth siRNA obtained from Life Technologies, Inc. We used MISSION siRNA universal as the negative control (Sigma). Cells were transfected with these siRNAs using Lipofectamine RNAiMAX (Life Technologies, Inc.), according to the manufacturer's instructions.

Cellular Oxygen Consumption and Measurement of Complex Activity in Intact Cells—The oxygen consumption rate (OCR) was determined using a Seahorse Extracellular Flux Analyzer XF24 (Seahorse Bioscience, North Billerica, MA). After transfection with siRNAs, HEPA-1 cells were cultured overnight in high-glucose DMEM. The cells were then dispersed and plated on a Seahorse 24-well plate at 1.2×10^4 cells/well and cultured overnight with 25 mM galactose, 1 mM pyruvate, 2 mM glutamine, and 10% FBS. The OCR was determined using the Seahorse Analyzer at each step before and after sequential injections of 0.5 μM oligomycin, 4 μM carbonyl cyanide *p*-trifluoromethoxyphenylhydrazone, and 1 μM rotenone/myxothiazol. To assay the activity of individual mitochondrial complexes, cells were permeabilized with XF Plasma Membrane Permeabilizer Reagent (Seahorse Bioscience) in mitochondrial assay solution buffer (Seahorse Bioscience) just before the assay. Respiration was assessed in the presence of 10 mM pyruvate (complex I substrate), 2 mM malate and 4 μM carbonyl cyanide *p*-trifluoromethoxyphenylhydrazone for complex I activity, and sequential addition of 2 μM rotenone (complex I inhibitor) and 10 mM succinate (complex II substrate) for complex II activity, then addition of 4 μM antimycin A (complex III inhibitor) for complex III activity, and final addition of 0.1 mM tetramethyl-*p*-phenylenediamine dihydrochloride containing 10 mM ascorbate (complex IV substrate) for complex IV activity. Complex III respiration was assessed after addition of 4 μM antimycin A. Cellular protein content was measured using a BCA protein assay kit (Thermo Scientific), and all results were normalized per total micrograms of protein.

Western Blotting Analysis—Anti-StarD7 antibody was prepared as reported previously (9). Other primary antibodies are as follows: total OXPHOS rodent WB antibody mixture (Abcam, Cambridge, UK) for complexes; rabbit anti-actin (Sigma); anti-optic atrophy 1 (Opa1) clone18/OPA1 (BD Transduction Laboratories); and anti-succinate dehydrogenase complex iron sulfur subunit A (SDHA) (Cell Signaling Technology). Cells were lysed in 20 mM Tris-HCl buffer (pH 8.0) containing 0.5% Triton X-100, 1 mM EDTA, 0.5 mM PMSF, and 5 μg/ml leupeptin, antipain, and chymostatin; protein was measured using a BCA protein assay kit.

To perform Western blotting analyses, proteins separated by SDS-PAGE were transferred to nitrocellulose membranes (Amersham Biosciences Protran, GE Healthcare) using a Trans-Blot SD Semi-Dry Transfer blotter (Bio-Rad), and the membranes were incubated with 5% (w/v) skim milk in TBS for 1 h and washed three times with T-TBS (TBS containing 0.02% Tween 20). The membranes were then incubated with antibodies overnight at 4 °C, washed three times with T-TBS, and incubated with horseradish peroxidase-conjugated IgGs for 1 h at room temperature. The membranes were washed three times with T-TBS and stained with a Clarity Western ECL substrate (Bio-Rad), according to the manufacturer's instructions, and visualized using a ChemiDoc MP (Bio-Rad). Protein band intensity was measured using Quantity One software (Bio-Rad). Data were obtained at the linear range of signal intensity. The band intensity was normalized against that of β-actin.

Generation of StarD7-KO HEPA-1 Cells by Double Nicking Using CRISPR-Cas9n—Genome editing of HEPA-1 cells was performed using a double-nicking approach that requires the activity of two nickase Cas9 enzymes (29). Two pairs (B1 and B2) of 20-bp single-guide RNAs (sgRNAs) targeting exon 1 of mouse *StarD7* were designed using the CRISPR design tool, available on line. The sgRNA pairs were cloned into a pSpCas9n(BB)-2A-Puro (PX462) vector (Addgene plasmid 48141). The sgRNA pairs were mStarD7-B1s (5′-CACC-GAAACAGAGGCATGGCCGGGG-3′) and mStarD7-B1r (5′-AAACCCCCGGCCATGCCTCTGTTTC-3′) (position, chromosome 2: 127,270,797), and mStarD7-B2s (5′-CAC-CGCGCTCTCCGGTGTTTTCGTA-3′) and mStarD7-B2r (5′-AAACTACGAAAACACCGGAGAGCGC-3′) (position, chromosome 2: 127,270,840). These vectors were co-transfected into HEPA-1 cells using Lipofectamine 2000 transfection reagent (Life Technologies, Inc.), according to the manufacturer's instructions. Forty eight hours after transfection, the cells were cultured in the presence of 5 μg/ml puromycin for 10 days, and surviving cells were then seeded as single colonies (0.5 cells/well) in 96-well plates. Single clones were expanded and screened for StarD7 expression by Western blotting, as described above. The genomic DNA from clones with a significant reduction in StarD7 expression was isolated using a standard proteinase K/phenol method, and the DNA fragments for the sgRNA target regions were amplified by PCR using one set of primers (mSD7g-checkF1, 5′-CTCCTCGGA-AGCCACGCTACCTCAGCCGCTTCTGC-3′, and mSD7g-checkR1, 5′-GCATCGTACTCAAAAGACCACTGGGCA-AACTGGGC-3′). PCR products were purified using a QIAquick gel extraction kit (Qiagen, Hilden Germany) and sequenced directly to verify the deletion mutation regions.

Isolation of Mitochondria from Cells—Mitochondria were isolated from HEPA-1 cells using a hybrid Percoll-metrizamide gradient method described by Storrie *et al.* (30). We substituted Nycodenz for metrizamide because the latter was difficult to obtain. Briefly, cells were homogenized by 80 strokes of a Dounce homogenizer in lysis buffer (20 mM Tris-HCl buffer (pH 8.0), 250 mM sucrose, 1 mM EGTA), and the homogenate was then centrifuged at $1,500 \times g$ for 5 min to remove nuclei and unbroken cells. The post-nuclear supernatant was applied to a hybrid Percoll/Nycodenz discontinuous density gradient (6% Percoll, 17% Nycodenz, 35% Nycodenz) and centrifuged at $50,000 \times g$ for 30 min using a Hitachi RPS40T rotor. The mitochondrion-rich bands were collected and diluted 10-fold with

lysis buffer. After centrifugation at 13,000 × *g* for 10 min, mitochondria were collected as the pellet.

Lipid Extraction and Quantification of Phospholipids by LC-MS/MS—Phospholipids were extracted from gradient-purified mitochondria (20 μg of protein) according to the Bligh and Dyer method (31). Briefly, 2 ml of methanol and 2 ml of chloroform were added to the purified mitochondria, followed by vortexing. Next, 2 μg of internal standards (1,2-dipentadecanoyl-PC and 1,2-diheptadecanoyl-PE from Avanti Polar Lipids, Alabaster, AL) and 1.8 ml of water were added, and the sample was vortexed again. The lower phase, containing total lipids, was dried under N_2 gas and then dissolved in methanol. Lipids were analyzed by reverse-phase ultra-high pressure liquid chromatography using an Acquity UPLC BEH C18 column (1.7 μm, 2.1 × 50 mm) (Waters, Milford, MA) coupled to a 5500 QTRAP mass spectrometer (Sciex Inc., Framingham, MA). A binary gradient consisting of solvent A (acetonitrile/methanol/water (1:1:3) containing 5 mM ammonium acetate) and solvent B (2-propanol containing 5 mM ammonium acetate) was used. The gradient profile was as follows: 0–1 min, 95% A; 1–9 min, 5–95% B linear gradient; 9–13 min, 95% B. The flow rate was 0.3 ml/min, and the column temperature was 40 °C. Quantification of individual lipid molecular species was performed using multiple reaction monitoring. Individual lipids were quantified using MultiQuant, version 2.0 (Sciex), and normalized against the internal standards. For the quantification of absolute amount of the major PC and PE species in mitochondria, PC (18:0–18:1 and 16:0–18:1) and PE (18:0–20:4) were obtained from Avanti Polar Lipids, and standard curves for these lipids were prepared.

Measurement of Cytochrome c Oxidase Activity—The enzyme assay for cytochrome *c* oxidase is based on a decrease in absorbance at 550 nm of ferrocytochrome *c* caused by its oxidation to ferricytochrome *c* by cytochrome *c* oxidase. Briefly, gradient-purified mitochondria were freeze-thawed and incubated with 20 μM reduced equine heart cytochrome *c* (Sigma) in 10 mM phosphate buffer (pH 7.5). The absorbance at 550 nm was determined using a Varioskan multimode microplate reader (Thermo Scientific). The activity was calculated using an extinction coefficient of 19.0 $mmol^{-1}\ cm^{-1}$.

Transfection of StarD7-KO Cells with Wild Human StarD7 (Rescue Experiment)—StarD7-KO cells were transfected with a plasmid encoding the genes for human StarD7-I or -II (pCAGGS-hStarD7-I or -II) (9) using Lipofectamine 2000, according to the manufacturer's instructions. StarD7-I has an N-terminal mitochondrial targeting sequence, whereas StarD7-II does not. For measurement of ATP production and cell growth rate, cells were cultured in high-glucose DMEM for 2 days after transfection with wild human StarD7 and then cultured in glucose-free DMEM containing 25 mM galactose for another 1 or 4 days. ATP level and cell growth rate were measured as described below. For Western blotting, cells were cultured in high-glucose DMEM at least 3 days after transfection, and the levels of MTCO1 and StarD7 protein were analyzed by Western blotting as described above.

Measurement of Cellular ATP Level and Growth Rate—Cells were cultured in high-glucose DMEM or glucose-free DMEM containing 25 mM galactose for 1 day. Cellular ATP was determined by luciferin-luciferase assay using an ATP assay kit (Toyo Ink, Tokyo, Japan), according to the manufacturer's instructions. The luminous intensity was measured using a luminometer (GloMax 20/20, Promega, Madison, WI) and normalized to the protein content.

To analyze cell growth rate, 5×10^3 cells were plated in wells of a 96-well plate and cultured in high-glucose DMEM or glucose-free DMEM containing 25 mM galactose. The cell proliferation rate was determined using a Cell Counting Kit-8 (Dojindo, Kumamoto, Japan), according to the manufacturer's protocol. The spectrophotometric absorbance in living cells was measured at a wavelength of 450 nm using a microplate spectrophotometer.

Quantitative Real Time (RT)-PCR of Respiratory Complex IV Subunits and TFAM—Total RNA was isolated from cells using an RNeasy mini kit (Qiagen) and treated with DNase (RNase-free DNase Set, Qiagen). The RNA was then reverse-transcribed using ReverTra Ace qPCR RT Master Mix (TOYOBO, Osaka, Japan), according to the manufacturer's instructions. Quantitative RT-PCR was carried out on a 7300 Real Time PCR System (Applied Biosystems) using FastStart Universal SYBR Green Master (Roche Applied Science). β-Actin was used as an internal control for verification. The following primers were used for qPCR (32): 5′-TCGGAGCCCCAGATATAGCA-3′, 5′-TTTCCGGCTAGAGGTGGGTA-3′ for MTCO1; 5′-CAAGGCCACCACACTCCTAT-3′, 5′-ATTCCTGTTGGAGGTCAGCA-3′ for MTCO3; 5′-CAAGTCAGCTGATGGGTATGG-3′, 5′-TTTCCCTGAGCCGAATCATCC-3′ for TFAM; and 5′-CATCCGTAAAGACCTCTATGCCAAC-3′, 5′-ATGGAGCCACCGATCCACA-3′ for β-actin.

Mitochondrial DNA (mtDNA)—Total DNA was isolated using a standard proteinase K/phenol method. The copy number of mtDNA (NADH dehydrogenase 1, ND1) and nuclear DNA platelet endothelial cell adhesion molecule-1 (PECAM-1) was determined by qRT-PCR using FastStart SYBR Green Master (Roche Applied Science) with a 7300 Real Time PCR System (Applied Biosystems). The following primers were used: 5′-CCTATCACCCTTGCCATCAT-3′, 5′-GAGGCTGTTGCTTGTGTGAC-3′ for ND1, and 5′-ATGGAAAGCCTGCCATCATG-3′, 5′-TCCTTGTTGTTCAGCATCAC-3′ for PECAM-1 (33). For the standards curves, a series of 10-fold dilutions of the plasmid DNA with an inserted target gene were generated, and the copy number of sample was determined.

Blue Native PAGE—Mitochondria were isolated from the cells by using a mitochondria isolation kit (Thermo Fisher Scientific), according to the manufacturer's instructions. Solubilization of mitochondria and BN-PAGE was performed as described before (14). Briefly, 400 μg of mitochondria were solubilized in 40 μl of 50 mM imidazole HCl (pH 7.0) containing 50 mM NaCl, 2 mM 6-aminohexanoic acid, 1 mM EDTA, and then added 12 μl of 20% digitonin (w/v) (digitonin/protein ratio of 6.0 g/g), kept on ice for 10 min. After centrifugation at 20,000 × g for 20 min, the supernatant was recovered. Then 5 μl of 50% glycerol (w/v) and 6 μl of 5% Coomassie Blue G-250 (w/v) suspended in 500 mM 6-aminohexanoic acid were added to the supernatant. Acrylamide native gel with 3–12% acrylamide gradient was prepared by using a gradient maker (Sanplatec Corp., Japan), and a sample of 20 μl was loaded onto each well. After

electrophoresis, gel was soaked in transfer buffer (25 mM Tris-HCl (pH 8.0), 0.1% SDS, 190 mM glycine, and 20% methanol) for 10 min, and protein was transferred to PVDF membrane. The blot was proved with anti-total OXPHOS rodent WB antibody mixture, and the protein band was visualized as described above.

Electron Microscopy—Cells were cultured in high-glucose DMEM and fixed in PBS containing 2% glutaraldehyde for 90 min at 4 °C. The cells were then rinsed thoroughly with PBS, post-fixed in 1% osmium tetroxide for 1 h at 4 °C, dehydrated in ethanol, and embedded. Ultrathin sections were stained with uranyl acetate followed by lead nitrate. Transmission electron microscopic images were obtained using a JEM-1210 microscope (JEOL, Tokyo, Japan).

Analysis of Opa1 Oligomerization—Opa1 oligomerization was analyzed as described before (13). Briefly, after washing with PBS, cells were treated with 1 mM bismaleimidohexane (Thermo Fisher Scientific), a cell-permeable cross-linker, for 20 min at 37 °C. After cross-linking, cells were washed twice in PBS containing 0.1% β-mercaptoethanol to quench the reaction. Cells were lysed, and prepared samples were separated with 5% acrylamide gel and subjected to Western blotting analysis as described above.

Statistical Analysis—Values are expressed as means ± S.D. Group means were compared using the Student's *t* test after analysis of variance to determine the significance of differences between individual means. A p value of <0.05 was considered indicative of statistical significance.

Author Contributions—Y. H. designed, performed, and analyzed the results of experiments and wrote the manuscript. M. I., H. A., and C. A. provided technical assistance. P. Z., L. V., and K. R. contributed to the Seahorse analyzer experiment. H. S. provided support in the design and performance of experiments and edited the manuscript. All authors read and approved the manuscript.

Acknowledgments—We thank Dr. Takashi Namatame (Clinical Research Center, Dokkyo University School of Medicine) for DNA sequencing and Dr. Masaru Tsumuraya (Department of Anatomic and Diagnostic Pathology, Dokkyo University School of Medicine) for electron microscopy analyses. We also thank the Research Support Center at Dokkyo University School of Medicine for allowing us to use its facilities.

References

1. Voelker, D. R. (2003) New perspectives on the regulation of intermembrane glycerophospholipid traffic. *J. Lipid Res.* **44,** 441–449
2. Vance, J. E. (2015) Phospholipid synthesis and transport in mammalian cells. *Traffic* **16,** 1–18
3. Daum, G. (1985) Lipids of mitochondria. *Biochim. Biophys. Acta* **822,** 1–42
4. Kornmann, B., Currie, E., Collins, S. R., Schuldiner, M., Nunnari, J., Weissman, J. S., and Walter, P. (2009) An ER-mitochondria tethering complex revealed by a synthetic biology screen. *Science* **325,** 477–481
5. de Brito, O. M., and Scorrano, L. (2008) Mitofusin 2 tethers endoplasmic reticulum to mitochondria. *Nature* **456,** 605–610
6. Filadi, R., Greotti, E., Turacchio, G., Luini, A., Pozzan, T., and Pizzo, P. (2015) Mitofusin 2 ablation increases endoplasmic reticulum-mitochondria coupling. *Proc. Natl. Acad. Sci. U.S.A.* **112,** E2174–E2181
7. Szabadkai, G., Bianchi, K., Várnai, P., De Stefani, D., Wieckowski, M. R., Cavagna, D., Nagy, A. I., Balla, T., and Rizzuto, R. (2006) Chaperone-mediated coupling of endoplasmic reticulum and mitochondrial Ca^{2+} channels. *J. Cell Biol.* **175,** 901–911
8. Iwasawa, R., Mahul-Mellier, A. L., Datler, C., Pazarentzos, E., and Grimm, S. (2011) Fis1 and Bap31 bridge the mitochondria-ER interface to establish a platform for apoptosis induction. *EMBO J.* **30,** 556–568
9. Horibata, Y., and Sugimoto, H. (2010) StarD7 mediates the intracellular trafficking of phosphatidylcholine to mitochondria. *J. Biol. Chem.* **285,** 7358–7365
10. Alpy, F., and Tomasetto, C. (2005) Give lipids a START: the StAR-related lipid transfer (START) domain in mammals. *J. Cell Sci.* **118,** 2791–2801
11. Clark, B. J. (2012) The mammalian START domain protein family in lipid transport in health and disease. *J. Endocrinol.* **212,** 257–275
12. Flores-Martin, J., Rena, V., Angeletti, S., Panzetta-Dutari, G. M., and Genti-Raimondi, S. (2013) The lipid transfer protein StarD7: structure, function, and regulation. *Int. J. Mol. Sci.* **14,** 6170–6186
13. Patten, D. A., Wong, J., Khacho, M., Soubannier, V., Mailloux, R. J., Pilon-Larose, K., MacLaurin, J. G., Park, D. S., McBride, H. M., Trinkle-Mulcahy, L., Harper, M. E., Germain, M., and Slack, R. S. (2014) OPA1-dependent cristae modulation is essential for cellular adaptation to metabolic demand. *EMBO J.* **33,** 2676–2691
14. Wittig, I., Braun, H. P., and Schägger, H. (2006) Blue native PAGE. *Nat. Protoc.* **1,** 418–428
15. Belenguer, P., and Pellegrini, L. (2013) The dynamin GTPase OPA1: more than mitochondria? *Biochim. Biophys. Acta* **1833,** 176–183
16. Cogliati, S., Frezza, C., Soriano, M. E., Varanita, T., Quintana-Cabrera, R., Corrado, M., Cipolat, S., Costa, V., Casarin, A., Gomes, L. C., Perales-Clemente, E., Salviati, L., Fernandez-Silva, P., Enriquez, J. A., and Scorrano, L. (2013) Mitochondrial cristae shape determines respiratory chain supercomplexes assembly and respiratory efficiency. *Cell* **155,** 160–171
17. Cipolat, S., Rudka, T., Hartmann, D., Costa, V., Serneels, L., Craessaerts, K., Metzger, K., Frezza, C., Annaert, W., D'Adamio, L., Derks, C., Dejaegere, T., Pellegrini, L., D'Hooge, R., Scorrano, L., and De Strooper, B. (2006) Mitochondrial rhomboid PARL regulates cytochrome *c* release during apoptosis via OPA1-dependent cristae remodeling. *Cell* **126,** 163–175
18. Frezza, C., Cipolat, S., Martins de Brito, O., Micaroni, M., Beznoussenko, G. V., Rudka, T., Bartoli, D., Polishuck, R. S., Danial, N. N., De Strooper, B., and Scorrano, L. (2006) OPA1 controls apoptotic cristae remodeling independently from mitochondrial fusion. *Cell* **126,** 177–189
19. Schenkel, L. C., and Bakovic, M. (2014) Formation and regulation of mitochondrial membranes. *Int. J. Cell Biol.* **2014,** 709828
20. Sharpley, M. S., Shannon, R. J., Draghi, F., and Hirst, J. (2006) Interactions between phospholipids and NADH:ubiquinone oxidoreductase (complex I) from bovine mitochondria. *Biochemistry* **45,** 241–248
21. Girdlestone, J., Bisson, R., and Capaldi, R. A. (1981) Interaction of succinate-ubiquinone reductase (complex II) with (arylazido)phospholipids. *Biochemistry* **20,** 152–156
22. Valpuesta, J. M., Goñi, F. M., Alonso, A., Arrondo, J. L., and Macarulla, J. M. (1988) Lipid-protein interactions. The mitochondrial complex III-phosphatidylcholine-water system. *Biochim. Biophys. Acta* **942,** 341–352
23. Tasseva, G., Bai, H. D., Davidescu, M., Haromy, A., Michelakis, E., and Vance, J. E. (2013) Phosphatidylethanolamine deficiency in mammalian mitochondria impairs oxidative phosphorylation and alters mitochondrial morphology. *J. Biol. Chem.* **288,** 4158–4173
24. Ellens, H., Siegel, D. P., Alford, D., Yeagle, P. L., Boni, L., Lis, L. J., Quinn, P. J., and Bentz, J. (1989) Membrane fusion and inverted phases. *Biochemistry* **28,** 3692–3703
25. Chernomordik, L., Kozlov, M. M., and Zimmerberg, J. (1995) Lipids in biological membrane fusion. *J. Membr. Biol.* **146,** 1–14
26. Osman, C., Voelker, D. R., and Langer, T. (2011) Making heads or tails of phospholipids in mitochondria. *J. Cell Biol.* **192,** 7–16
27. Yang, L., Lewkowich, I., Apsley, K., Fritz, J. M., Wills-Karp, M., and Weaver, T. E. (2015) Haploinsufficiency for Stard7 is associated with enhanced allergic responses in lung and skin. *J. Immunol.* **194,** 5635–5643
28. Fritz, J. M., Yang, L., and Weaver, T. E. (2015) Lipid transport and epithelial barrier integrity. *Oncotarget* **6,** 20744–20745
29. Ran, F. A., Hsu, P. D., Lin, C. Y., Gootenberg, J. S., Konermann, S., Trevino, A. E., Scott, D. A., Inoue, A., Matoba, S., Zhang, Y., and Zhang, F. (2013)

Double nicking by RNA-guided CRISPR Cas9 for enhanced genome editing specificity. *Cell* **154,** 1380–1389
30. Storrie, B., and Madden, E. A. (1990) Isolation of subcellular organelles. *Methods Enzymol.* **182,** 203–225
31. Bligh, E. G., and Dyer, W. J. (1959) A rapid method of total lipid extraction and purification. *Can. J. Biochem. Physiol.* **37,** 911–917
32. Jousse, C., Muranishi, Y., Parry, L., Montaurier, C., Even, P., Launay, J. M., Carraro, V., Maurin, A. C., Averous, J., Chaveroux, C., Bruhat, A., Mallet, J., Morio, B., and Fafournoux, P. (2014) Perinatal protein malnutrition affects mitochondrial function in adult and results in a resistance to high fat diet-induced obesity. *PLoS ONE* **9,** e104896
33. Mitsuhashi, S., Hatakeyama, H., Karahashi, M., Koumura, T., Nonaka, I., Hayashi, Y. K., Noguchi, S., Sher, R. B., Nakagawa, Y., Manfredi, G., Goto, Y., Cox, G. A., and Nishino, I. (2011) Muscle choline kinase β defect causes mitochondrial dysfunction and increased mitophagy. *Hum. Mol. Genet.* **20,** 3841–3851